EXPERIMENTAL INVESTIGATION ON THE INFLUENCE OF CASING RELATIVE MOTION ON HEAT TRANSFER CHARACTERISTICS OF THE SQUEALER TIP

Ziqiang LI, Pingting CHEN*, Yuming SHAO, Feng HAN

College of Energy and Power Engineering, Nanjing University of Aeronautics and Astronautics.
No.29, Yudao Street, Nanjing, Jiangsu, 210000, P.R. China

* Corresponding author; E-mail: cpt09@nuaa.edu.cn

Abstract: This study develops an experimental setup for turbine blade-casing relative motion investigation and employing transient liquid crystal thermometry for precise thermal measurements, and systematically examines the coupled effects of tip clearance height with squealer rim dimensions (height and width) and Reynolds number (Re) on heat transfer characteristics of the squealer tip under the casing relative motion. The experimental results were fitted with empirical formulas.The results demonstrated that the relative motion between the turbine blade and the casing altered the heat transfer distribution while reducing the heat transfer coefficient at the blade tip. For instance, increasing the casing velocity from 0 m/s to 30 m/s decreased the area-averaged heat transfer coefficient at the squealer tip by 10.93%, with a more pronounced reduction of 17.19% observed at the squealer rim top surface. Under casing relative motion, increasing the height and width of the squealer rim significantly reduces heat transfer coefficient and enhances the uniformity of the heat transfer distribution. For instance, increasing the squealer rim height from 1.5% to 5.0% of the blade height reduced the area-averaged heat transfer coefficient by approximately 20.0%, while expanding the squealer rim width from 1.0% to 4.0% of the blade height decreased the area-averaged heat transfer coefficient by 10.64%. Increasing the tip clearance height from 1.0% to 3.0% of the blade height elevated the heat transfer coefficient by 5.5% to 7.4%, confirming that smaller tip clearance height favor heat transfer coefficient reduction. Higher Re increased the heat transfer coefficient, though the growth rate diminished progressively with increasing Re.

Key words*: casing relative motion, squealer tip, squealer rim dimension, blade tip heat transfer, coupling effect*

1. Introduction

High-pressure turbines are critical components in aeroengines, where maintaining radial clearance between rotating blades and stationary casings is essential for operational safety. However, pressure-driven high-temperature gas penetration through this clearance causes severe thermal erosion at blade tips, significantly impacting service life and reliability [1]. Understanding heat transfer characteristics in this region is therefore vital for engineering applications.

Compared to flat tips, squealer tips effectively suppress tip leakage flows and reduce thermal loads, making them widely adopted in blade tip design[2-3].Krishnababu et al. [4] demonstrated that squealer tips reduce averaged heat transfer coefficients by near 9% compared to flat tips. Key influencing factors include tip clearance height, inflow conditions, and squealer rim geometry (such as height/width) [5]. Azad et al. [6] experimentally observed increased heat transfer coefficients with larger tip clearances in static cascades. Chen et al. [7] and Arisi et al. [8] linked elevated Mach and Reynolds numbers to intensified heat transfer peaks on squealer bottoms. Nasir et al. [9] reported a 25% reduction in averaged heat transfer coefficients by increasing rim height from 1.0% to 4.2% of blade height using transient liquid crystal thermometry. Kwak et al. [10] and numerical studies [11-12] confirmed that taller rims reduce both heat transfer coefficients and high-heat-flux areas. Senel et al. [13] identified enhanced cavity effects and reduced heat transfer with narrower rim, though Li et al. [14] cautioned that an excessively narrow rim increase localized heat flux despite improving aerodynamic efficiency. These findings highlight the multi-parametric nature of squealer tip heat transfer characteristics [15].

Prior studies [6,8-11,13-15] primarily examine static blade-casing configurations, neglecting relative motion between rotating blades and casings inherent in real turbine operation [16-17]. Recent numerical work highlights motion-induced effects: Krishnababu et al. [18] observed reduced tip heat transfer under casing motion, while Zhu et al. [19] and Jiang et al. [20] identified altered aerothermal responses, including 10% heat transfer reduction and bottom's mid-arc high-heat-flux streaks. Zhou et al. [21] attributed Nusselt number redistribution to scraping vortices from transonic end-wall motion, with rim height dominating over width variations. Experimental validations [22-23] confirmed motion-induced leakage flow modifications and more than 10% averaged Nusselt number reduction by using large-scale linear cascades. Lu et al. [24-25] employed high-speed rotating disks with infrared thermography to quantify enhanced heat transfer uniformity in squealer fore-regions under casing motion, suggesting thermal load alleviation mechanisms [26-27].While numerical simulations dominate this field [18-21], experimental data remain scarce, particularly regarding localized thermal load characteristics and multi-factor coupling effects under relative motion.

Addressing these gaps, this study develops a novel experimental apparatus simulating blade-casing relative motion through controlled casing rotation. Furthermore, transient liquid crystal thermometry is employed to systematically investigate the heat transfer distribution and variation characteristics at the tip clearance height in coupled with the squealer rim height, width, and Reynolds number (*Re*), all influenced by the casing's motion. This research elucidates the effect of the casing relative motion and the coupling of multiple factors on the heat transfer at the squealer tip, and fits empirical formulas for the influence of various factor on the heat transfer coefficient at the squealer tip, providing valuable benchmarks for future studies on heat transfer at the blade tip.

2. Instructions

2.1. Test rig

The experimental apparatus adopts the rotating disk-type casing motion concept by Lu et al. [24–25] (Figure 1). The test section features a five-blade, four-passage linear cascade and a ultra-clear glass casing driven by a variable-frequency motor. The moving casing has a diameter of 1.30 meters and a thickness of 19.0 mm. The effective sweeping radius of the casing is 0.6 meters, and its vertical vibration displacement is limited to less than ±0.05 mm. The casing rotates counterclockwise (from the blade suction side to the blade pressure side) to simulate blade-casing relative motion.A compliant brush seal minimizes leakage at the cascade-casing interface.

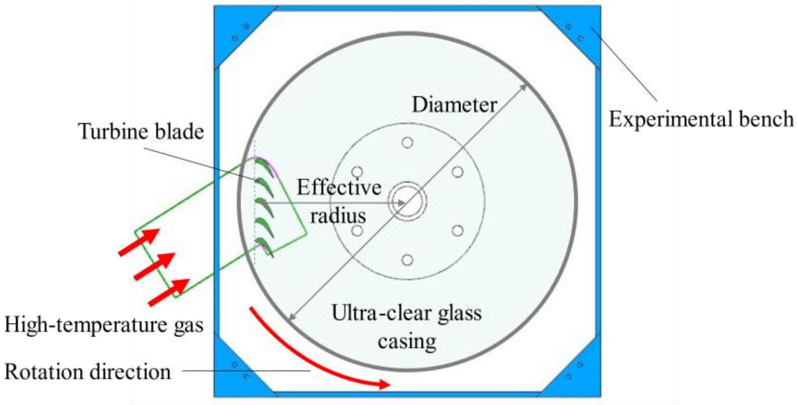

Fig. 1 Layout of the test section with turbine blade and casing

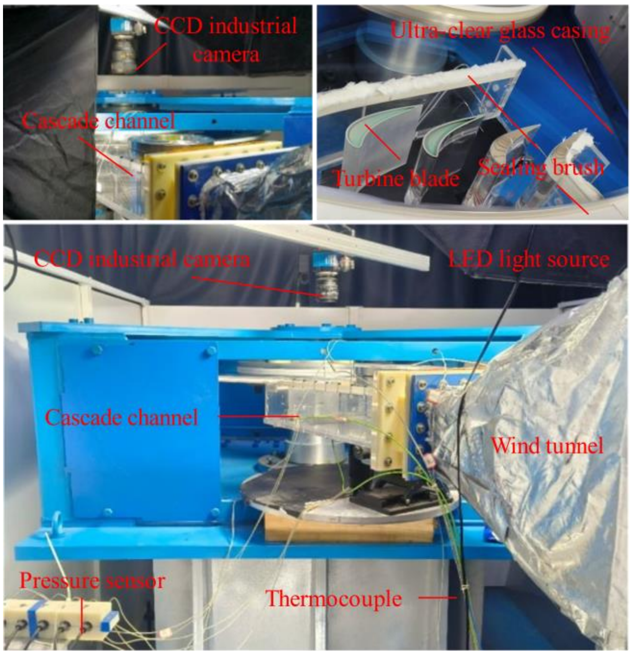

Fig. 2 The actual experimental device for relative motion between the turbine blade and casing

The cascade employs a scaled-up (2.5 times) GE-E^3 high-pressure turbine first-stage rotor blade as the reference model (straight blade, no distortion) with a height (S) of 102.5 mm. Acrylic blades with low thermal conductivity enable precise tip heat transfer measurements and accommodate the size of the casing.

2.2. Experimental Measurement and Transient Liquid Crystal Calibration

The volumetric flow rate in the cascade passage is measured using a vortex flowmeter. Thermocouples positioned at the inlet, outlet, and blade tip regions record temperature data via an MT-X inspection instrument. Total and static pressures at the cascade inlet/outlet are acquired using Omega pressure sensors integrated with an NI LabVIEW data acquisition system.

Heat transfer coefficients on the squealer tip surface are quantified via transient liquid crystal (TLC) thermometry through optical visualization. Thermochromic liquid crystals (40–60°C range, RGB color response) are applied to the blade tip, with a pre-calibrated hue-temperature relationship (Figure 3) enabling temperature field reconstruction. During testing, a CCD camera (91.5% light transmittance through the ultra-clear glass casing) captures TLC color distributions. A MATLAB-based algorithm extracts localized hue values, interpolates data, and maps temperatures using the calibration curve.

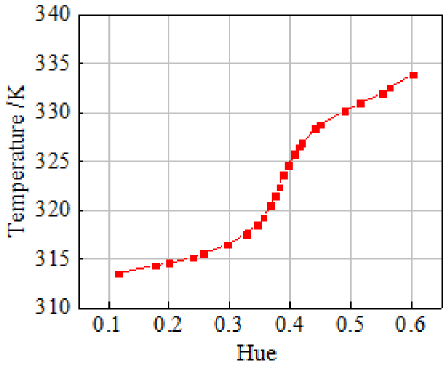

Fig. 3 Corresponding curve of liquid crystal Hue and Temperature

The turbine blades, fabricated from low thermal conductivity material (λ = 0.16 W m^{-1} K^{-1}), adhere to unsteady-state one-dimensional semi-infinite heat conduction theory. The heat transfer coefficient (*HTC*) is derived from the surface temperature evolution[28]:

$$\frac{T_\tau - T_0}{T_\infty - T_0} = 1 - \exp\left(\frac{HTC^2 a\tau}{\lambda^2}\right) \times \mathrm{erfc}\left(\frac{HTC\sqrt{a\tau}}{\lambda}\right) \tag{1}$$

Where, T_∞, T_0, and T_τ represent incoming flow, initial blade tip surface, and τ time- blade tip surface temperatures, respectively. τ corresponds to liquid crystal discoloration time, a is the thermal diffusion coefficient of the blade material, and λ is the thermal conductivity of the blade material.

2.3. Accuracy verification of test rig

Experimental validation utilized published data from Oxford University's moving belt facility studies [23, 29]. Geometric and dynamic similarity principles ensured equivalence in blade cascade inlet velocity triangles and outlet Reynolds numbers. Heat transfer measurements were performed on scaled turbine blade models using a moving ultra-clear glass casing assembly. For the convenience of comparison, only the *Nu* distribution region was retained in the blade tip of references [23,29], and the same treatment was done in the *Nu* distribution region of the heat transfer experiment in this study. Figures 4 and 5 showed the *Nu* contour distribution and axial distribution in the balde tip region, respectively. Notably, the area-averaged *Nu* values in Figure 4 was equal to the axially-averaged values presented in Figure 5.

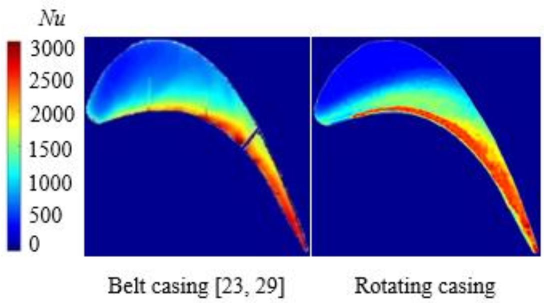

Fig. 4 Distribution of Nusselt numbers at the blade tip

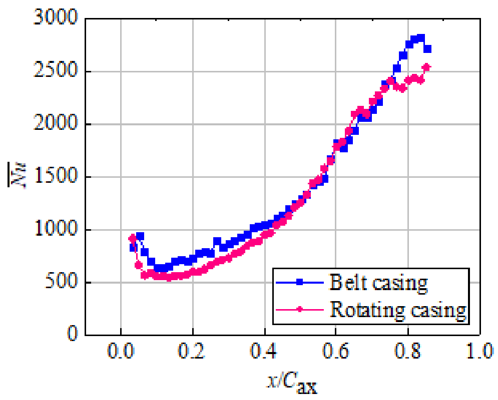

Fig. 5 Axial distribution of Nusselt number

(The belt casing is experimental data published by references [23,29], and the rotating casing is experimental data in this study. x is the axial position of the blade, and C_{ax} is the axial chord length of the blade.)

Results align with Oxford's data: low *Nu* at the suction-side's mid-front edge and high *Nu* from the pressure side to trailing edge, with similar axial distribution. Moreover, the averaged *Nu* obtained in the present experiments were 6.21% lower than those reported in references [23,29], confirming the new experimental device can accurately to capture resolve blade tip heat transfer characteristics.

2.4. Experimental measurement error analysis

Heat transfer measurements are subject to multiple uncertainty sources, introducing potential deviations between experimental and true values. To quantify errors and validate reliability, uncertainty analysis was applied. Transient liquid crystal thermometry uncertainties primarily arise from temperature and time measurement inaccuracies, along with material property variations. Using error propagation theory [30], *HTC* uncertainty was calculated through functional relationships.

The dimensionless parameters included in the *HTC* equation are:

$$\psi = \frac{T_w - T_0}{T_g(\tau) - T_0}, \quad \sigma = \frac{HTC}{\sqrt{\rho_s c_s \lambda_s}} \tag{2}$$

Furthermore, based on the one-dimensional thermal conductivity equation, it is derived that:

$$\psi = 1 - \exp(\sigma^2 \tau)\operatorname{erfc}(\sigma\sqrt{\tau}) \tag{3}$$

According to equations 2, the uncertainty of the *HTC* can be derived:

$$\frac{dHTC}{HTC} = \sqrt{\left(\frac{d\sigma}{\sigma}\right)^2 + \left(\frac{1}{2}\frac{d\tau}{\tau}\right)^2 + \left(\frac{1}{2}\frac{d(\rho_s c_s \lambda_s)}{\rho_s c_s \lambda_s}\right)^2} \tag{4}$$

The uncertainty caused by measurement time and material properties can be ignored, and the uncertainty of the *HTC* can be simplified as:

$$\frac{dHTC}{HTC} = \phi_{HTC}\left(dT / \left(T_g(\tau) - T_0\right)\right) \tag{5}$$

When the excess temperature ψ in the above dimensionless parameters is in the range of 0.3~0.7, the scaling factor $\emptyset_{HTC}$ is relatively small and can be taken as 5.0. In this experiment, the uncertainty dT/T of the temperature is ± 0.1 K, and $T_g(\tau) - T_0$ is in the range of 5.0~10.0 K. Therefore, the uncertainty of the *HTC* is 5.0%~10.0%.

2.5. Experimental conditions and Tested blade tip configurations

The casing's relative motion velocity (v = 30 m/s) in the experiment was derived from the turbine blade velocity triangle, corresponding to twice the incoming flow velocity [31]. The cascade outlet Reynolds number (Re) is 2.0×10^5 was calculated using the flow velocity and blade chord length. Inlet conditions included a turbulence intensity of 5.25% and a stabilized temperature of 335 K, with the cascade outlet exposed to atmospheric pressure. Two tip clearance heights (δ = 1.0% S and 3.0% S, where S denotes the blade height, S = 102.5 mm) were tested. Experimental parameters and squealer rim geometries are detailed in Table 1.

Tab. 1 Experimental conditions and squealer rim's dimensions

Case number	Casing's velocity	Tip clearance height	Re	Rim height	Rim width
0	0 m/s	1.0% S	2.0×10^5	3.0% S	2.0% S
1	30 m/s	1.0% S	2.0×10^5	1.5% S	2.0% S
2	30 m/s	3.0% S	2.0×10^5	1.5% S	2.0% S
3	30 m/s	1.0% S	2.0×10^5	3.0% S	2.0% S
4	30 m/s	3.0% S	2.0×10^5	3.0% S	2.0% S
5	30 m/s	1.0% S	2.0×10^5	5.0% S	2.0% S
6	30 m/s	3.0% S	2.0×10^5	5.0% S	2.0% S
7	30 m/s	1.0% S	2.0×10^5	3.0% S	1.0% S
8	30 m/s	3.0% S	2.0×10^5	3.0% S	1.0% S
9	30 m/s	1.0% S	2.0×10^5	3.0% S	4.0% S
10	30 m/s	3.0% S	2.0×10^5	3.0% S	4.0% S
11	30 m/s	1.0% S	1.6×10^5	3.0% S	2.0% S
12	30 m/s	3.0% S	1.6×10^5	3.0% S	2.0% S
13	30 m/s	1.0% S	2.4×10^5	3.0% S	2.0% S
14	30 m/s	3.0% S	2.4×10^5	3.0% S	2.0% S

This study first investigates the influence of casing relative motion on the heat transfer characteristics of the squealer tip under specified tip clearance heights and squealer rim dimensions (height/width). Subsequently, based on a prescribed relative casing motion velocity, it systematically examines the combined effects of large and small tip clearance heights coupled with variations in squealer rim dimensions (height/width) and Re on the thermal behavior of the squealer tip.

3. Result and Analysis

3.1. Effects of casing relative motion on squealer tip heat transfer characteristics

Figure 6 illustrates the HTC distribution across the squealer tip configuration, comprising both the squealer bottom surface and rim top surface, under stationary casing (NRMC, Case 0) and casing-blade relative motion (RMC, Case 3) conditions.

Under stationary casing conditions, the squealer bottom surface exhibits distinct regional variations: Region A at the leading edge demonstrates elevated HTC levels due to leakage flow impingement, while the trailing edge maintains comparatively lower heat transfer intensity. In contrast, the squealer rim top surface displays enhanced heat transfer characteristics with substantially higher *HTC*. Notably, the leading edge and suction side of the squealer rim, influenced by leakage flow inlet/outlet effects, demonstrate markedly elevated HTC that exceed those observed at the pressure side and trailing edge of the rim.

When the casing motion relative to the turbine blades, Region A experiences both reduced *HTC* magnitude and spatial contraction of the high-heat transfer zone. A distinct high-*HTC* stripe emerges parallel to the pressure-side edge of the squealer rim, extending along the mid-arc line from the leading edge to mid-chord position (Region B) [20]. Concurrently, the *HTC* at the rim top surface diminishes, with the significant reduction observed at the mid-front edge of the suction-side (Region C). Despite these changes, the leading edge and mid-rear edge of the suction side remain high-*HTC* zones.

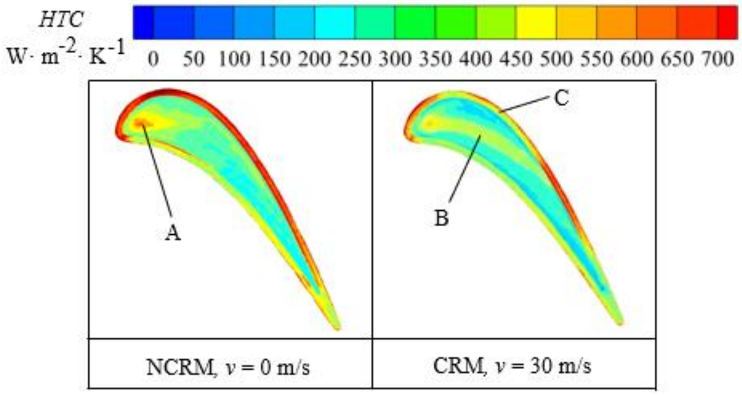

Fig. 6 Distribution of *HTC* at the squealer tip with or without relative motion of the casing

Figure 7 illustrates the axial *HTC* distribution, along with the entire and partial area-averaged *HTC* of the squealer tip.

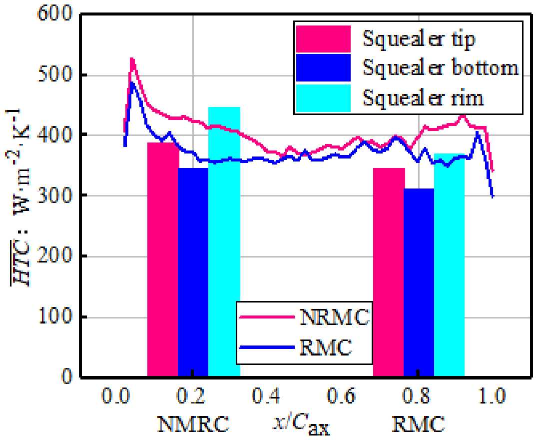

Fig. 7 The axial *HTC* distribution as well as the entire and partial area-averaged *HTC* of the squealer tip

Compared to the stationary casing condition, casing motion reduces the area-averaged *HTC* across both the entire squealer tip and its sub-regions. Specifically, the area-averaged *HTC* decreases by 10.93% for the entire squealer tip, 10.25% for the squealer bottom, and 17.19% for the squealer rim top surface. Casing motion exerts a more pronounced suppression effect on heat transfer at the squealer rim. The squealer rim exhibits a 1.3 times higher area-averaged *HTC* than the bottom, underscoring its vulnerability to thermal loads.

Axially, the *HTC* distribution displays a characteristic oscillatory pattern: an initial increase, followed by sequential decreases, subsequent increases, and a final decline. The leading edge maintains higher *HTC* than mid-chord and trailing regions. The observed *HTC* reduction under casing motion is particularly significant at the mid-front and trailing edges, a phenomenon associated with suppressed *HTC* distribution along the suction-side rim in these regions.

3.2. Effects of squealer rim height on squealer tip heat transfer characteristics

Figure 8 presents the *HTC* distribution at the squealer tip under casing relative motion, considering coupled variations in tip clearance height (δ) and squealer rim height (h) (Cases 1–6).

When δ = 1.0% *S*, *h* = 1.5% *S*, a high-*HTC* stripe parallel to the pressure-side edge of the rim forms from the leading edge to the near mid-arc of the squealer bottom, while other areas exhibit low *HTC*. The leading edge and the mid-rear edge of the rim's suction side are regions with significantly higher *HTC* than the squealer bottom and the pressure side. Increasing *h* to 3.0% *S* reduces *HTC* across both the squealer bottom and rim, confining high *HTC* to the rim's leading edge and mid-rear suction side. At *h* = 5.0% *S*, no distinct heat transfer stripes form on the squealer bottom, with high *HTC* localized at the rim leading edge, resulting in markedly reduced and uniform *HTC*.

When δ increases to 3.0% *S* and *h* remains at 1.5% *S*, the heat transfer stripe on the near mid-arc of the squealer bottom shortens, yet the *HTC* increases substantially, particularly at the leading edge and the suction side of the squealer rim. For *h* of 3.0% *S* and 5.0% *S*, the *HTC* distribution at the squealer tip resembles that observed at *h* = 1.5% *S*, but with lower *HTC* and poorer heat transfer uniformity.

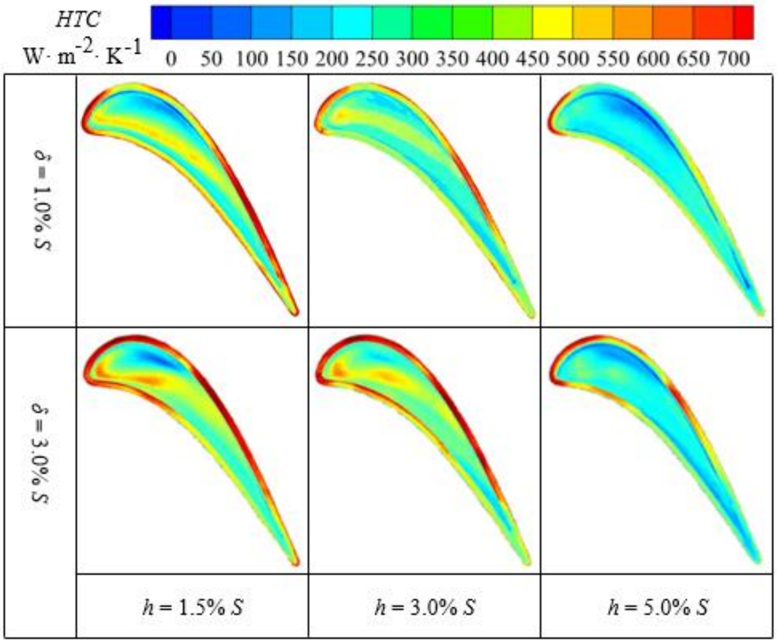

Fig. 8 Distribution of *HTC* at the squealer tip of different squealer rim heights

Figure 9 presents the area-averaged *HTC* of the squealer tip under coupled variations in δ and *h*. The area-averaged *HTC* decreases with increasing *h*. Compared with the increase of *h* from 1.5% *S* to 3.0% *S*, the decrease of the squealer tip's area-averaged *HTC* increases significantly from 3.0% S to 5.0% S, reaching 19.55%. Under the casing relative motion, the area-averaged *HTC* of the squealer tip corresponding to the smaller tip clearance height decreases more greatly, which is more conducive to decrease heat load. As the δ increases, the area-averaged *HTC* increases nearly 5.5%.

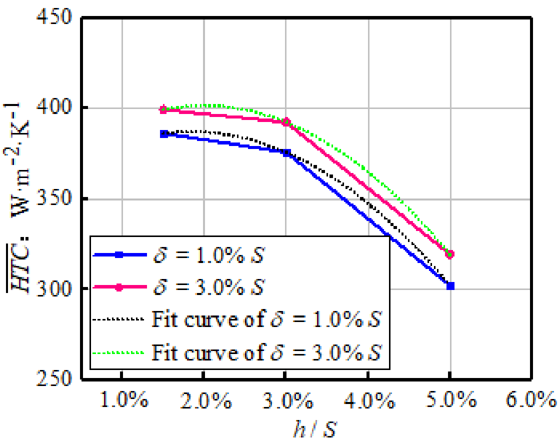

Fig. 9 Area-averaged *HTC* and the fit curve of different squealer rim heights

Based on the variation characteristics of the area-averaged *HTC*, the empirical formula on the experimental results is fitted. As shown in Table 2.

Tab. 2 Empirical formula of area-averaged *HTC* with tip clearance height and rim height

Formula	$HTC = B_1{*}(h / S)^2 + B_2{*}(h / S) + \text{Intercept}$	
δ	δ = 1.0% S	δ = 3.0% S
B_1	-85028.59	-91042.68
B_2	3130.26	3633.42
Intercept	358.32	365.19

Figure 10 compares the area-averaged *HTC* of the squealer rim and squealer bottom at δ = 1.0% S. Both surfaces exhibit declining *HTC* with increasing h, accompanied by a 53% reduction in their *HTC* disparity between h = 1.5% S and 5.0% S. This trend highlights improved heat transfer uniformity at the squealer tip. At h = 5.0% S, the *HTC* distribution becomes low and uniform, effectively mitigating thermal loads.

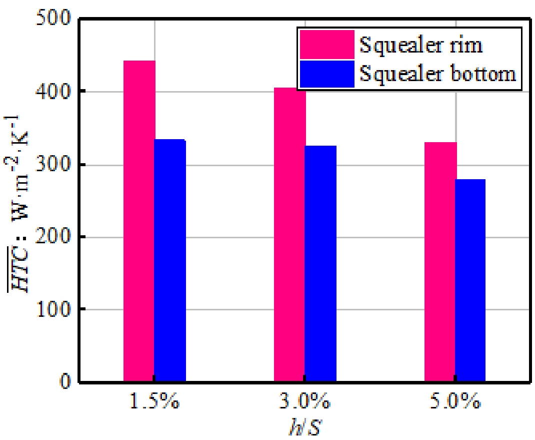

Fig. 10 Averaged *HTC* of squealer rim and squealer bottom under different squealer rim heights

The *HTC* at the squealer tip with h = 5.0% S is low and evenly distributed, leading to weakened heat transfer and a lower tip heat load.

3.3. Effects of squealer rim width on squealer tip heat transfer characteristics

Figure 11 depicts the *HTC* distribution at the squealer tip under casing relative motion, considering coupled variations in tip clearance height (δ) and squealer rim width (w) (Cases 3, 4, 7-10).

For δ = 1.0% *S* and w = 1.0% *S*, high-*HTC* fringes parallel to the pressure-side edge form at the squealer bottom mid-arc. Compared to the squealer bottom, the squealer rim is divided into regions with high *HTC*, with the highest values occurring at the rim's leading edge. Increasing w to 2.0% *S* diminishes mid-arc *HTC* fringes, leaving elevated *HTC* only at the suction-side's leading and mid-rear edges. At w = 4.0% *S*, high-*HTC* regions nearly vanish, yielding a uniform low-*HTC* distribution.

When δ increases to 3.0% *S*, the *HTC* of both the squealer bottom and rim increases proportionally, expanding the spatial extent of high-*HTC* regions. Notably, the *HTC* with w = 4.0% *S* decreases significantly, while high *HTC* is scattered in the leading edge and the mid-rear edge of the rim's suction side, worsening the heat transfer uniformity at the tip.

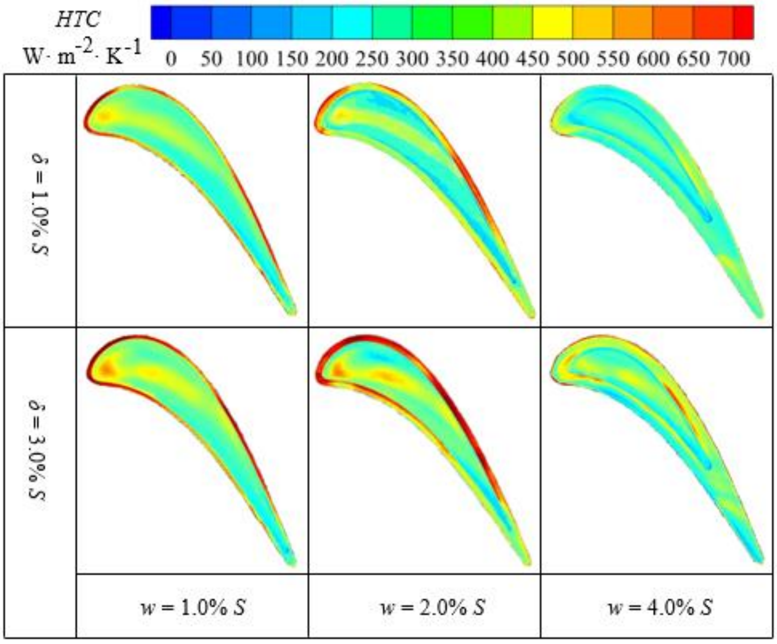

Fig. 11 Distribution of *HTC* at the squealer tip of different squealer rim widths

Figure 12 illustrates the area-averaged *HTC* of the squealer tip under coupled effects of δ and w during casing relative motion.

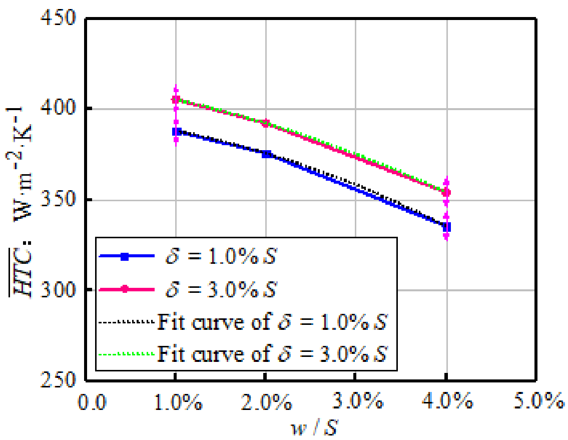

Fig. 12 Area-averaged *HTC* and the fit curve of different squealer rim widths

The area-averaged *HTC* of the squealer tip decreases with an increase in *w*. For *w* of 1.0% *S* to 2.0% *S*, the area-averaged *HTC* of the squealer tip increases slightly, followed by a decrease of 0.45% to 1.55%. At *w* = 4.0% *S*, the area-averaged *HTC* of the squealer tip increases. With increasing δ, the area-averaged *HTC* increases by 5.58% to 7.40%.

The empirical formula obtained by fitting the experimental results is shown in Table 3.

Tab. 3 Empirical formula of area-averaged *HTC* with tip clearance height and rim width

Formula	$HTC = B_1*(w/S)^2 + B_2*(w/S)$ + Intercept	
δ	δ = 1.0% *S*	δ = 3.0% *S*
B_1	-26018.10	-19665.68
B_2	-446.16	-718.70
Intercept	395.03	414.49

Figure 13 compares area-averaged *HTC* for the squealer rim and bottom at δ = 1.0% *S*. Increasing *w* reduces *HTC* disparities by nearly 60%, confirming improved uniformity. Configurations with *w* = 4.0% *S* achieve minimal *HTC* gradients, particularly at smaller tip clearance height .

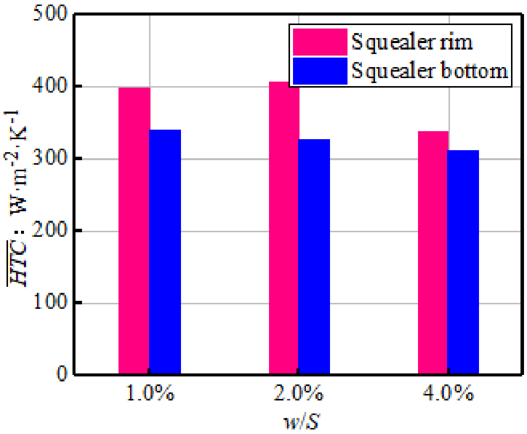

Fig. 13 Area-averaged *HTC* of squealer rim and squealer bottom under different squealer rim widths

As *w* increases, the *HTC* decreases significantly. Particularly, *w* = 4.0% *S* has no significant high *HTC* distribution, especially showing more uniform heat transfer distribution with δ = 1.0% *S*.

3.4. Effects of Reynolds number on squealer tip heat transfer characteristics

Figure 14 illustrates the *HTC* distribution at the squealer tip under casing relative motion, considering coupled variations in tip clearance height (δ) and Reynolds number (*Re*) (Cases 3, 4, 11-14).

At δ = 1.0% *S* and *Re* = 1.6×10^5, distinct high heat transfer regions form along the mid-arc of the squealer's bottom surface. Comparative analysis reveals elevated *HTC* at the leading edge and mid-rear edge of the suction side relative to other blade tip regions. When δ = 3.0% *S*, the heat transfer zone contracts longitudinally while exhibiting significant *HTC* intensification. Under this configuration, the leading edge and suction side of the squealer rim emerge as primary high-*HTC* regions, contrasting with reduced *HTC* observed along the pressure side and trailing edge. As the *Re* increases from 1.6×10^5 to 2.0×10^5 and then to 2.4×10^5, the *HTC* distribution at the squealer tip remains similar to that at *Re* = 1.6×10^5, with a significant increase in *HTC* at corresponding positions.

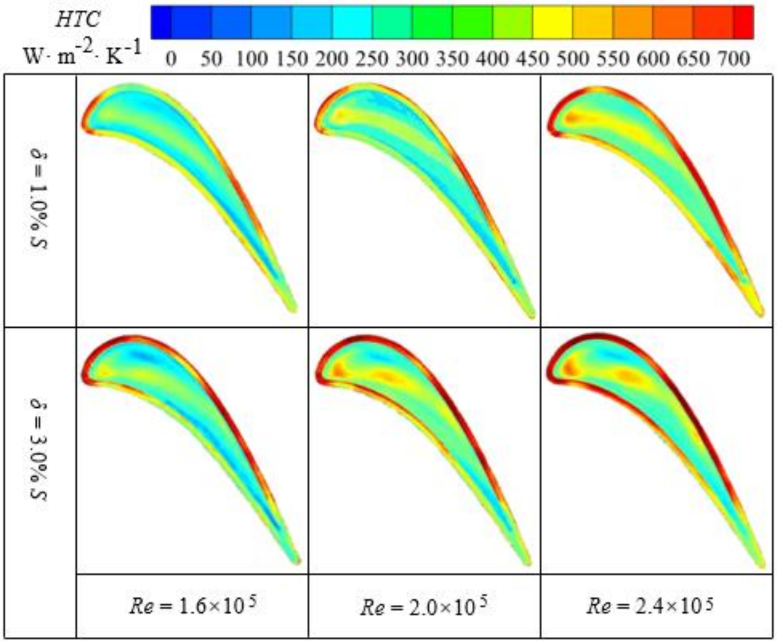

Fig. 14 Distribution of *HTC* at the tip of different *Re*

Figure 15 demonstrates the coupled effects of δ and *Re* on area-averaged *HTC*. *HTC* increases by 4.03% to 10.54% as *Re* rises from 1.6×10^5 to 2.4×10^5, with diminishing growth rates. Concurrently, increasing δ from 1.0% *S* to 3.0% *S* elevates *HTC* by nearly 6.50%.

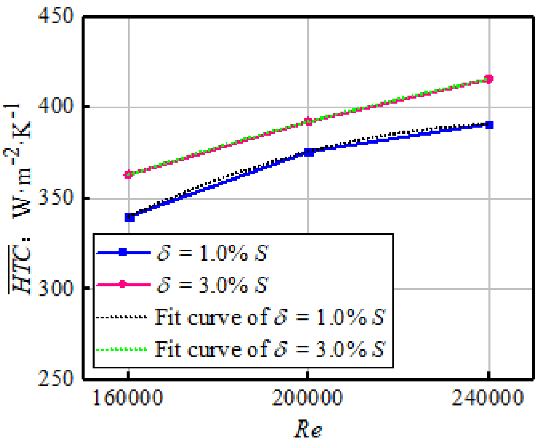

Fig. 15 Area-averaged *HTC* and the fit curve of different *Re*

The empirical formula obtained by fitting the experimental results is shown in Table 4.

Tab. 4 Empirical formula of area-averaged *HTC* with tip clearance height and *Re*

Formula	$HTC = B_1 * Re^2 + B_2 * Re$ + Intercept	
δ	δ = 1.0% *S*	δ = 3.0% *S*
B_1	-6.46E-9	-1.84E-9
B_2	0.00322	0.00139
Intercept	-10.06	187.12

The *HTC* at the squealer tip increases with the *Re* increase under the casing relative motion, and the *HTC* distribution patterns remain similar across different *Re*.

4. Conclusions

This study systematically investigated the effects of casing relative motion on the heat transfer characteristics of the squealer tip. Subsequently, experimental studies were conducted to analyze the coupled effects of tip clearance height (δ) with rim height (h), width (w), and Reynolds number (Re) on the heat transfer performance under casing relative motion. The conclusions are as follows:

1) The casing relative motion reduces *HTC* of the squealer tip while altering the heat transfer distribution. High-*HTC* streaks parallel to the pressure-side rim are observed near the mid-arc of the squealer bottom. Casing velocity increases from 0 m/s to 30 m/s, the area-averaged *HTC* of the squealer tip, squealer bottom, and squealer rim decreases by 10.93%, 10.25%, and 17.19%, respectively.

2) Increasing δ from 1.0% S to 3.0% S under relative motion raises the area-averaged *HTC* of the squealer tip by nearly 7.40%, accompanied by increased *HTC* distribution heterogeneity. Smaller tip clearance height is more favorable for reducing both *HTC* and thermal load.

3) The area-averaged *HTC* of the squealer tip decreases with increasing h. When h increases from 1.5% S to 5.0% S, the area-averaged *HTC* decreases by nearly 20.0%, and the *HTC* uniformity improves significantly, particularly under smaller tip clearance height.

4) Expanding w reduces the *HTC* and enhances distribution uniformity. Compared to w = 1.0%S, increasing w to 4.0% S results in a 10.6% reduction in area-averaged *HTC*, with the disappearance of localized high *HTC* regions. Within the studied range, w = 4.0% S exhibits optimal thermal performance.

5) Increasing Re elevates the *HTC* of the squealer tip. As Re rises from 1.6×10^5 to 2.4×10^5, the area-averagedd *HTC* increases by 4.03% to 10.54%. However, the growth rate diminishes with higher Re, indicating reduced sensitivity to further Reynolds number escalation.

Acknowledgment

The authors gratefully acknowledge the financial supports for the project from National Major Science and Technology Projects of China (Grant No. J2019-I-0004-0005) and National Nature Science Foundation of China (grant No.:52106047).

References

[1] R, S, Bunker., Axial turbine blade tips: function, design, and durability, *Journal of propulsion and power, 22* (2006), 2, pp. 271–285

[2] Ameri, A. A., *et al*., Effect of squealer tip on rotor heat transfer and Efficiency, *Journal of Turbomachinery, 120* (1998), 4, pp. 753–759

[3] Lee, S. W., Chae, B. J., Effects of squealer rim height on aerodynamic losses downstream of a high-turning turbine rotor blade, *Experimental Thermal and Fluid Science, 32* (2008), 8, pp. 1440–1447

[4] Krishnababu, S. K., *et al*., Aerothermal investigations of tip leakage flow in axial flow turbines-Part I: Tip geometry and tip clearance gap, *Journal of Turbomachinery, y, 131* (2009), 1, 011006

[5] Gao, J., *et al*., Research progress on turbine blade tip aerodynamics and heat transfer technology for gas turbines, *Acta Aeronautica et Astronautica Sinica, 38* (2017), 9, pp. 76-106

[6] Azad, G., S., *et al*., Heat Transfer and Flow on the Squealer Tip of a Gas Turbine Blade, *Journal of Turbomachinery, 122,* (2000), 4, pp. 725-732

[7] Chen, S., *et al*., The aerothermal performance of turbine blade squealer tip at various Reynolds numbers and Mach numbers with moving end-wall, *International Journal of Turbo & Jet-Engines, 40* (2023), 1, 0040

[8] Arisi, A., *et al*., An Experimental and Numerical Study on the Aerothermal Characteristics of a Ribbed Transonic Squealer-Tip Turbine Blade with Purge Flow, *Journal of Turbomachinery, 138* (2016), 10, 101007

[9] Nasir, H., *et al*., Effect of tip gap and squealer geometry on detailed heat transfer measurements over a high-pressure turbine rotor blade tip, *Journal of Turbomachinery,126* (2004), 2, pp. 221-228

[10] Kwak, J., S., *et al*., Effects of rim location, rim height, and tip clearance on the tip and near tip region heat transfer of a gas turbine blade, *International Journal of Heat and Mass Transfer, 47* (2004), 26, pp. 5651-5663

[11] Huang, T., *et al*., Influences of depth and rim width of squealer tip on the leakage flow and heat transfer, *Global Power and Propulsion Society,* (2021), pp.1-8

[12] Bi, S., *et al*., Effect of Squealer Tip with Deep Scale Depth on the Aero-thermodynamic Characteristics of Tip Leakage Flow, *Journal of Thermal Science,31* (2022), pp.1773-1789

[13] Senel, C., B., *et al*., An aerothermal study of the influence of squealer width and height near a HP turbine blade, *International Journal of Heat and Mass Transfer 120* (2018), pp. 18-32

[14] Li, J., *et al*., Effects of tip cavity geometries on the aerothermal performance of the transonic turbine blade with cavity tip, *Journal of Power and Energy, 230* (2016), 3, pp. 319-331

[15] Azad, G., S., *et al*., Effect of squealer geometry arrangement on a gas turbine blade tip heat transfer, *ASME Journal of Heat Transfer, 124* (2002), pp. 452-459

[16] Yang, D., Feng, Z., Tip leakage flow and heat transfer predictions for turbine blades, *ASME Turbo Expo: Power for Land, Sea, and Air,* (2007), pp. 589-596

[17] Yang, D., *et al*., Investigation of Leakage Flow and Heat Transfer in a Gas Turbine Blade Tip with Emphasis on the Effect of Rotation, *Journal of Turbomachinery,132* (2010), 4,pp. 1-9

[18] Krishnababu, S., K., *et al*., Aerothermal Investigations of Tip Leakage Flow in Axial Flow Turbines—Part II: Effect of Relative Casing Motion, *Journal of Turbomachinery,131* (2009), 1,pp. 69-78

[19] Zhu, D., *et al*., Relative casing motion effect on squealer tip cooling performance at tight tip clearance, *Journal of Thermal Science and Engineering Applications,* (2020), pp. 1-18

[20] Jiang, S., *et al*., Numerical Investigations on the Heat Transfer Performance of Transonic Squealer Tip with Different Film Cooling Layouts, ASME Turbo Expo 2020: Turbomachinery Technical Conference and Exposition, 2020

[21] Zhou, C., Effects of end-wall motion on thermal performance of cavity tips with different squealer width and height, *International Journal of Heat and Mass Transfer, 91* (2015), pp. 1248-1258

[22] Palafox, P., *et al*., PIV Maps of Tip Leakage and Secondary Flow Fields on a Low-Speed Turbine Blade Cascade with Moving End-wall, *Journal of Turbomachinery,130* (2008),1, 011001

[23] Palafox, P., *et al*., Blade Tip Heat Transfer and Aerodynamics in a Large-Scale Turbine Cascade with Moving End-wall, *Journal of Turbomachinery,134* (2012), 2, 021020

[24] Lu, S., *et al*., A High-Speed Disk Rotor Rig Design for Tip Aerothermal Research, Turbo Expo: Power for Land, Sea, and Air. *American Society of Mechanical Engineers*, 2020, 84188

[25] Lu, S, *et al*., A High-Speed Disk Rotor Rig Design for Tip Aerothermal Research, *Journal of Turbomachinery,144* (2022), 5, 051002

[26] Xie, W., *et al*., Experimental Study of Turbine Blade Tip Heat Transfer with High-Speed Relative Casing Motion, *Proceedings of the Global Power and Propulsion Society,* Xi'an, China, 2021, pp.18-20

[27] Xie, W., *et al*., Interaction Mechanism of Transonic Squealer Tip Cooling with the Effect of High-Speed Relative Casing Motion, *Journal of Turbomachinery,145* (2023), 8, 081016

[28] Poser, R., Transient heat transfer experiments in complex geometries using liquid crystal thermography, Ph. D. thesis, University of Stuttgart, Stuttgart, Germany, 2010

[29] Tang, Brian. M. T., *et al*., Computational Modelling of Tip Heat Transfer to a Super-Scale Model of an Unshrouded Gas Turbine Blade, *American Society of Mechanical Engineers,* (2008), pp. 1063-1074

[30] Yan, Y. Y., Owen, J. M., Uncertainties in transient heat transfer measurements with liquid crystal, *International Journal of Heat and Fluid Flow, 23* (2002), 1, pp. 29-35

[31] Sumanta., *et al*., Numerical Study of the Flow Past a Turbine Blade Tip: Effect of Relative Motion Between Blade and Shroud, *Journal of turbomachinery, 136* (2014), 3, 031015

Paper submitted: 13 March 2025

Paper revised: 03 April 2025

Paper accepted: 15 May 2025